

Towards Better Alignment: Training Diffusion Models with Reinforcement Learning Against Sparse Rewards

Zijing Hu^{1*} Fengda Zhang^{2*} Long Chen³ Kun Kuang^{1†} Jiahui Li¹ Kaifeng Gao¹
Jun Xiao¹ Xin Wang⁴ Wenwu Zhu⁴

¹Zhejiang University, ²Nanyang Technological University, ³The Hong Kong University of Science and Technology, ⁴Tsinghua University
{zj.hu, fdzhang}@zju.edu.cn, zjuchenlong@gmail.com, {kunkuang, jiahui1, kite_phone}@zju.edu.cn,
junx@cs.zju.edu.cn, {xin-wang, wwzhu}@tsinghua.edu.cn

Abstract

Diffusion models have achieved remarkable success in text-to-image generation. However, their practical applications are hindered by the misalignment between generated images and corresponding text prompts. To tackle this issue, reinforcement learning (RL) has been considered for diffusion model fine-tuning. Yet, RL’s effectiveness is limited by the challenge of sparse reward, where feedback is only available at the end of the generation process. This makes it difficult to identify which actions during the denoising process contribute positively to the final generated image, potentially leading to ineffective or unnecessary denoising policies. To this end, this paper presents a novel RL-based framework that addresses the sparse reward problem when training diffusion models. Our framework, named B^2 -DiffuRL, employs two strategies: **Backward progressive training** and **Branch-based sampling**. For one thing, backward progressive training focuses initially on the final timesteps of denoising process and gradually extends the training interval to earlier timesteps, easing the learning difficulty from sparse rewards. For another, we perform branch-based sampling for each training interval. By comparing the samples within the same branch, we can identify how much the policies of the current training interval contribute to the final image, which helps to learn effective policies instead of unnecessary ones. B^2 -DiffuRL is compatible with existing optimization algorithms. Extensive experiments demonstrate the effectiveness of B^2 -DiffuRL in improving prompt-image alignment and maintaining diversity in generated images. The code for this work is available¹.

1. Introduction

The text-to-image generation task aims to produce images from textual descriptions, holding significant potential for

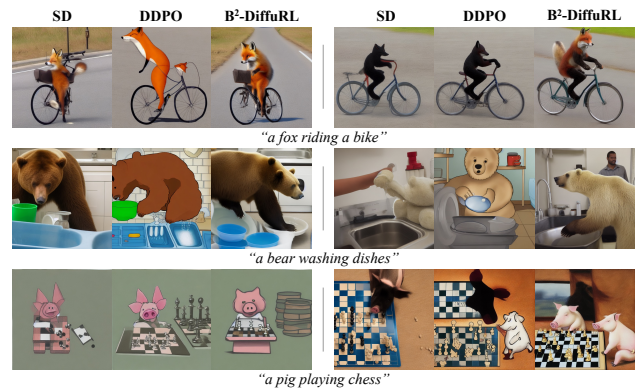


Figure 1. (**Prompt-image Misalignment**) Text-to-image diffusion models (e.g., Stable Diffusion (SD) [52]) may not generate high-quality images that accurately align with prompts. Existing reinforcement learning-based diffusion model fine-tuning methods (e.g., DDPO [8]) have limited effect and loss of image diversity. For each set of images above, we use the same seed for sampling.

various applications [49, 56]. Recently, diffusion models have garnered widespread attention due to their success in this domain [15, 23, 59]. These models employ a sequential denoising process that transforms random noise into detailed images. However, even the most advanced text-to-image diffusion models, such as DALLE3 [6] and Stable Diffusion [52], often encounter issues with misalignment between the generated images and the textual descriptions [28]. This misalignment limits the practicality and effectiveness of these models in real-world applications.

To solve this problem, recent studies have explored incorporating reinforcement learning (RL) techniques to fine-tune pre-trained text-to-image diffusion models [8, 17, 32, 46, 63, 65]. By formulating the step-by-step denoising process as a *sequential decision-making problem*, RL enables diffusion models to optimize for specific long-term objectives, beyond merely fitting to static data as done in standard supervised learning [29, 52, 64]. In this formulation, noisy images at different timesteps are viewed as *states* in RL, while denoising at each timestep corresponds to an *action*.

*Equal contribution. †Corresponding author.

¹<https://github.com/hu-zijing/B2-DiffuRL>.

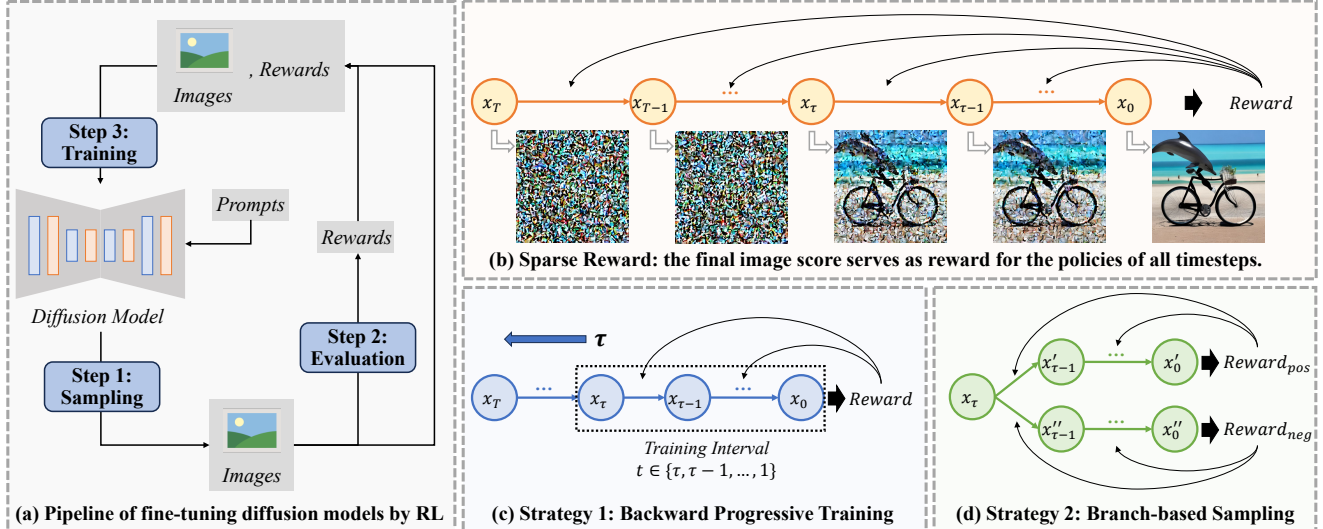


Figure 2. (**Sparse Reward**) When people train diffusion models with reinforcement learning (RL), the reward is only available at the end of the generation process. This sparsity limits the success of RL in diffusion models. We propose B^2 -DiffuRL, a new RL framework with two strategies, to mitigate this issue.

The alignment scores between the final generated images and the textual prompts, which can be derived from human preferences or model evaluations, serve as the *rewards*. The pipeline of training diffusion models with RL is illustrated in Figure 2 (a). Researchers first sample images using the diffusion model with given prompts and then calculate the alignment scores as rewards. These sampled trajectories, consisting of images at different timesteps and their corresponding alignment scores, can be used as training data for RL to further enhance the diffusion models [25].

However, RL has so far made limited success in improving prompt-image alignment, primarily due to the key challenge of *sparse reward*. As shown in Figure 2 (b), reward in this context is sparse because it is only available at the end of the generation process. Sparse rewards are harmful to RL-based diffusion fine-tuning in two ways:

- **Limited improvement in alignment.** The denoising actions at different timesteps focus on varying levels of semantics (e.g., early timesteps define layout, middle timesteps refine style, and late timesteps enhance detailed objects) and have different impacts on the final image [69, 70]. With sparse rewards, it is difficult to identify which actions during the denoising process contribute positively to the final alignment, so actions at different timesteps receive inappropriate rewards. As a result, learning effective policies becomes challenging.
- **Sacrificing diversity for better alignment.** To achieve higher alignment score, the model may learn unnecessary policies. For example, with prompts like “a bear washing dishes”, cartoon-like images are more likely to get higher rewards than realistic photographs because the prompts are often depicted in a cartoon style in pre-training data. With sparse rewards, model fine-tuned via naive RL al-

gorithms (e.g., DDPO [8]) may learn these unnecessary policies about styles, resulting in generating only cartoon-like images, as shown in Figure 1. This shows a trade-off between alignment and diversity, where alignment is improved at the expense of diversity [54, 72].

The challenge of sparse reward has attracted widespread attention in traditional RL [20, 62]. The classic solutions are constructing additional rewards by various techniques, such as reward shaping [40, 50], to achieve dense reward functions [13, 19, 27, 43]. Unfortunately, these solutions are not suitable for diffusion models because it is hard to evaluate the noisy images in the denoising process. This motivates us to ask: *How can we mitigate the negative effects of sparse rewards when using RL to train diffusion models?*

In this paper, we introduce a novel RL-based fine-tuning framework for diffusion-based text-to-image generation to address the challenge of sparse reward, which we refer to as B^2 -DiffuRL². Our framework employs two strategies. The first one is **backward progressive training** (BPT), applied to the training stage. Initially, we focus training on only the final timesteps of the image generation process, as shown in Figure 2 (c). As training rounds increase, we gradually extend the training interval backward to cover all timesteps, and achieve training on the entire denoising process in the end. The second strategy is **branch-based sampling** (BS), applied to the sampling stage. For each training interval in denoising process, we perform branch sampling to get multiple samples under each branch, as shown in Figure 2 (d). Within each branch, we only select the best and worst samples to form a contrastive sample pair for RL training.

² B^2 -DiffuRL is short for **B**ackward progressive training and **B**ranch-based sampling for **R**einforcement **L**earning in **D**iffusion models.

Our framework has the following three capabilities: (1) **Better prompt-image alignment.** With small training interval, BPT strategy enables the models to easily and quickly learn the policies for the later timesteps of generation. As the model becomes proficient in these later timesteps, it progressively learns to manage the earlier timesteps of the denoising process. By mitigating the complexity of dealing with the entire process from the outset, BPT reduces the learning difficulty associated with sparse rewards. Moreover, with BS strategy, the contrastive samples within the same branch share identical states and actions up to the start of the training interval. By comparing the contrastive samples, the models can accurately identify how much the denoising policies of the current training interval contribute to the final image during training. (2) **Maintaining diversity when improving alignment.** Denoised from the same intermediate state, the contrastive samples share similar coarse-grained visual information (e.g., image styles) but receive different rewards. It prevents the models from learning unnecessary policies (e.g., about image styles) as shortcuts to achieve high rewards, thus helping maintain diversity. (3) **Compatibility.** Although we mainly compare with the current state-of-the-art RL-based fine-tuning algorithm called DDPO [8] in this paper, our framework is compatible with any previous optimization algorithm such as policy gradient [57], DPO [48, 63] and DPOK [17]. Experiments show that applying B²-DiffuRL can improve effectiveness of different algorithms in terms of both alignment and diversity.

Our contributions can be summarized as: (1) We investigate the problem of RL-based diffusion models fine-tuning for improving prompt-image alignment, and for the first time highlight the challenge of sparse reward. (2) We propose a compatible RL-based fine-tuning framework named B²-DiffuRL, employing backward progressive training and branch-based sampling strategies, to address the above challenge. (3) Extensive experimental results on Stable Diffusion [52] show the effectiveness of B²-DiffuRL in terms of both alignment and diversity when compatible with different RL algorithms, without increasing computational cost.

2. Related Work

2.1. Text-to-Image Diffusion Models

Diffusion models have gained substantial attention for their ability to generate high-quality samples [23, 59, 60, 67]. One of the primary applications of diffusion models is image generation [5, 24]. These models have been shown to produce images that are both high in fidelity and diversity, rivaling the outputs of Generative Adversarial Networks (GANs) [15, 18]. The extension of diffusion models to text-to-image generation has opened up possibilities for creating images from textual descriptions [71]. Works like DALL-E [49] and Imagen [55] have demonstrated that

diffusion models can be effectively conditioned on textual input to produce corresponding images. Despite their success, text-to-image diffusion models often suffer from the issue of prompt-image misalignment [31, 44].

2.2. Reinforcement Learning with Sparse Reward

Reinforcement Learning (RL) is a learning paradigm in which an agent learns to make decisions by interacting with an environment to maximize cumulative rewards [29, 45]. Applications of RL span various domains, including gaming, robotics, finance, and healthcare [11, 39]. Recently, RL has played an important role in alignment. For example, RL has been leveraged to fine-tune large language models (LLMs), ensuring that the generated outputs align with human values and intentions [9]. One of the significant challenges in RL is dealing with sparse rewards, where feedback signals are infrequent and the agent must explore extensively to discover rewarding states [50, 62]. Traditional RL algorithms struggle in such settings due to the inefficiency in learning from limited feedback [20, 40]. Various techniques have been proposed to address this challenge [3, 42], such as reward shaping [13, 19, 27, 43], where additional heuristic rewards are provided to guide the agent. However, these classic RL strategies can not be applied to our problem directly, since it is difficult to evaluate the noisy images during denoising process.

2.3. Improving Alignment of Diffusion Models

Early diffusion models focused primarily on the quality and fidelity of the generated images [15, 23, 59]. However, as the demand for a more interactive and user-driven generation grew, improving alignment between prompts and generated images is crucial for enhancing the usability and reliability of these models in practical applications [16, 34, 53, 73]. The initial approaches to conditioning diffusion models on text prompts employ a variety of techniques, including both classifier guidance and classifier-free guidance [15, 22]. With the advent of LDMs [51], subsequent researches focus on fine-tuning pre-trained models to enhance alignment [26, 33]. Recently, RL has been employed to fine-tune the text-to-image diffusion models [8, 10, 17, 32, 46, 63, 65, 66, 68]. However, the issue of sparse rewards limits the performance of such methods in prompt-image alignment, and even sacrifices a lot of diversity in order to improve controllability. In this paper, by mitigating the negative effects of sparse rewards, we further develop the application of RL in training diffusion models.

3. Method

In this section, we first introduce how to train diffusion models with RL. Then we highlight the challenge of sparse reward in this context. Finally, we introduce

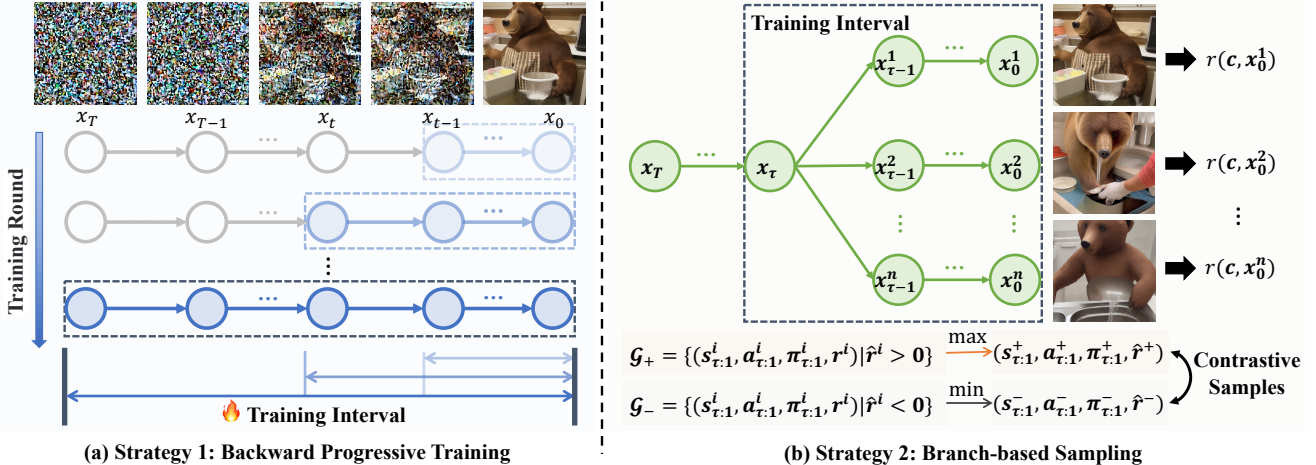


Figure 3. **(Method)** We propose the framework B²-DiffuRL, employing two strategies to address the challenge of sparse rewards. (a) Backward progressive training strategy: We focus initially on the final timesteps of the denoising process and gradually extend the training interval to earlier timesteps, easing the learning difficulty associated with sparse rewards. (b) Branch-based sampling strategy: We perform branch-based sampling at the beginning of each training interval. Comparisons between samples within the same branch provide a clear indication of whether the policies of the current training interval positively contribute to the final images.

B²-DiffuRL, employing two strategies to address this challenge. B²-DiffuRL can be compatible with different RL algorithms, such as DDPO [8], DPO [63] and DPOK [17].

3.1. Problem and Challenge

Text-to-Image Diffusion Models. Text-to-image diffusion models iteratively refine random noise into a coherent image that matches the given prompt [52]. The process of diffusion models consists of two phases: the forward process and the reverse process [23]. In the forward process, an image \mathbf{x}_0 is gradually corrupted into pure noise \mathbf{x}_T through T steps, where Gaussian noise is added at each step. The reverse process aims to generate an image from pure noise conditioned on a textual description \mathbf{c} by denoising iteratively [23, 58]:

$$p_{\theta}(\mathbf{x}_{t-1} \mid \mathbf{x}_t, \mathbf{c}) = \mathcal{N}(\mathbf{x}_{t-1}; \mu_{\theta}(\mathbf{x}_t, t, \mathbf{c}), \sigma_t \mathbf{I}^2), \quad (1)$$

where μ_{θ} is predicted by a diffusion model parameterized by θ , and σ_t is the fixed timestep-dependent variance.

Training Diffusion Models with RL. The denoising process of diffusion models can be formulated as a *sequential decision-making problem*. Therefore, this process can be viewed through the lens of RL, where each step in the denoising process is considered as a decision made by an agent (the diffusion model). Following this formulation, the *state* s_t at each timestep is represented by $(\mathbf{c}, t, \mathbf{x}_t)$, *i.e.*, the text prompt, the current timestep, and the noisy image at the current timestep. The sequence of states represents the gradual refinement from noise to the final image. The *action* a_t at each timestep involves denoising by sampling the next noisy image \mathbf{x}_{t-1} . The *policy* π_{θ} , parameterized

by θ , defines the action selection strategy. In this context, the policy is defined as $\pi_{\theta}(a_t \mid s_t) = p_{\theta}(\mathbf{x}_{t-1} \mid \mathbf{x}_t, \mathbf{c})$. The *reward* can be defined as a prompt-image alignment score $r(\mathbf{c}, \mathbf{x}_0) \in \mathbb{R}$, which is given by human preferences or model evaluations. A larger reward means a better prompt-image alignment. To improve the prompt-image alignment of diffusion models, we can execute RL-based training by maximizing the following objective:

$$\mathcal{J}_{\text{RL}}(\theta) = \mathbb{E}_{\mathbf{c} \sim p(\mathbf{c}), \mathbf{x}_0 \sim p_{\theta}(\mathbf{x}_0 \mid \mathbf{c})} [r(\mathbf{x}_0, \mathbf{c})], \quad (2)$$

where $p(\mathbf{c})$ follows a uniform distribution, meaning that we randomly sample prompts from a candidate set of prompts. To construct the training data for RL, we first collect denoising trajectories via sampling based on diffusion models. Then we can update parameters θ via gradient descent [41].

Challenge of Sparse Reward. However, the reward $r(\mathbf{x}_0, \mathbf{c})$ is only available at the end of the image generation process. This sparsity of reward makes it challenging for the diffusion model to identify which actions during the denoising process positively impact the final alignment and reward them appropriately. As a result, the diffusion model struggles to learn effective strategies and may even adopt unnecessary or incorrect ones. The classic RL strategies, such as constructing additional rewards, are not suitable here because it is difficult to evaluate the noisy images during the denoising process. This motivates us to develop new RL strategies for training diffusion models to mitigate the negative effects of sparse rewards. For a comprehensive discussion on the challenge of sparse reward, we refer the readers to Appendix C.

3.2. Strategy 1: Backward Progressive Training

The conventional training methods involve training the model across all timesteps of the denoising process from the beginning. However, due to the complexity and large noise present in the early timesteps, the training process can be unstable and inefficient, especially with sparse rewards. We hypothesize that focusing on the final timesteps, where the generated images are more coherent and less noisy, could provide a more stable foundation for the RL training. By mastering these final timesteps first, the model can incrementally handle the earlier, noisier stages more effectively, leading to overall better performance and control. We call this strategy as backward progressive training (BPT). Formally, let T represent the total number of timesteps in the denoising process. Initially, we train the model on the last τ timesteps, where $\tau < T$. Therefore, each trajectory sampled for training consists of τ timesteps:

$$\{s_t, a_t, \pi_\theta(a_t | s_t) | t = \tau, \tau-1, \dots, 1\} \text{ with reward } r(\mathbf{x}_0, \mathbf{c}), \quad (3)$$

which can be abbreviated as $(s_{\tau:1}, a_{\tau:1}, \pi_{\tau:1}, r)$ without ambiguity. As training progresses, the training interval is extended backward by incorporating more timesteps, ultimately covering the entire range from T to 1. The training objective during each phase remains consistent with Eq. (2). Following DDPO, we use policy gradient estimation [30, 57] and the gradient is:

$$\nabla_\theta \mathcal{J}_{\text{BPT}} = -\mathbb{E} \left[\sum_{t=1}^{\tau} \frac{p_\theta(\mathbf{x}_{t-1} | \mathbf{x}_t, \mathbf{c})}{p_{\theta_{\text{old}}}(\mathbf{x}_{t-1} | \mathbf{x}_t, \mathbf{c})} \nabla_\theta \log p_\theta(\mathbf{x}_{t-1} | \mathbf{x}_t, \mathbf{c}) \hat{r}(\mathbf{x}_0, \mathbf{c}) \right], \quad (4)$$

where θ_{old} is the parameters of diffusion model prior to update and \hat{r} is the normalized value of reward r (see Appendix D.1 for details). The expectation is taken over sampled denoising trajectories.

Previous works fine-tune diffusion models along the entire denoising process from x_T to x_0 , with the sparse reward r_0 . With such sparse reward, it is difficult for the model to directly learn effective network parameters for the entire denoising process. We propose BPT to make the model learn the denoising process from x_τ to x_0 first. As training progresses, τ is gradually increased to T , and the model learns to manage the earlier timesteps after becoming proficient in later timesteps. This is easier than directly learning the entire denoising process. By applying BPT, the model can more effectively learn how to denoise when only x_0 , state at the last timestep, has a reward. We refer the readers to Appendix C for a comprehensive discussion.

3.3. Strategy 2: Branch-based Sampling

The sparse rewards make it difficult to tell whether actions on certain timesteps during denoising have a positive or negative effect on the final alignment. To further mitigate this issue, we introduce the strategy of branch-based sam-

pling (BS). When constructing training data for RL, we perform branch sampling at the beginning of training interval $[\tau, 1]$, as shown in Figure 3 (b). Within each branch, we divide the sampled denoising trajectories (distinguished by the superscript i) into two groups:

$$\begin{aligned} \mathcal{G}_+ &= \{ (s_{\tau:1}^i, a_{\tau:1}^i, \pi_{\tau:1}^i, \hat{r}^i) | \hat{r}^i := \hat{r}(\mathbf{x}_0^i, \mathbf{c}) > 0 \}, \\ \mathcal{G}_- &= \{ (s_{\tau:1}^i, a_{\tau:1}^i, \pi_{\tau:1}^i, \hat{r}^i) | \hat{r}^i := \hat{r}(\mathbf{x}_0^i, \mathbf{c}) < 0 \}, \end{aligned} \quad (5)$$

where group \mathcal{G}_+ consists of trajectories with positive rewards (if available), and group \mathcal{G}_- consists of trajectories with negative rewards (if available). We then select the trajectory $(s_{\tau:1}^+, a_{\tau:1}^+, \pi_{\tau:1}^+, \hat{r}^+)$ with the best reward from the positive group and the trajectory $(s_{\tau:1}^-, a_{\tau:1}^-, \pi_{\tau:1}^-, \hat{r}^-)$ with the worst reward from the negative group to form a contrastive sample pair for RL. The gradient of the contrastive sample pair is:

$$\begin{aligned} \nabla_\theta \mathcal{J}_{\text{BS}} = -\mathbb{E} \left(\sum_{t=1}^{\tau} \left[\frac{p_\theta(\mathbf{x}_{t-1}^+ | \mathbf{x}_t^+, \mathbf{c})}{p_{\theta_{\text{old}}}(\mathbf{x}_{t-1}^+ | \mathbf{x}_t^+, \mathbf{c})} \nabla_\theta \log p_\theta(\mathbf{x}_{t-1}^+ | \mathbf{x}_t^+, \mathbf{c}) \hat{r}^+ \right. \right. \\ \left. \left. + \frac{p_\theta(\mathbf{x}_{t-1}^- | \mathbf{x}_t^-, \mathbf{c})}{p_{\theta_{\text{old}}}(\mathbf{x}_{t-1}^- | \mathbf{x}_t^-, \mathbf{c})} \nabla_\theta \log p_\theta(\mathbf{x}_{t-1}^- | \mathbf{x}_t^-, \mathbf{c}) \hat{r}^- \right] \right). \end{aligned} \quad (6)$$

By isolating the impact of actions outside the training interval on the final images, the comparison between the contrastive samples directly reflects how much the actions within the training interval contribute to the reward. Branch-based sampling strategy provides clear signals to the model, allowing the model to focus on actions that truly drive positive outcomes. Therefore, it further mitigates the impact of reward sparsity and facilitates more efficient learning of effective policies. Moreover, by avoiding learning unnecessary policies (*e.g.*, image styles), our approach can also maintain the diversity of generated images, which will be demonstrated and discussed in the following section. We emphasize that B²-DiffuRL does not increase computational cost of RL algorithms, as discussed in Appendix D.3.

4. Experiments

In this section, we evaluate the effectiveness of B²-DiffuRL in terms of improving prompt-image alignment and maintaining diversity. We first compare our method with existing state-of-the-art method DDPO [8]. Then, we focus on ablation studies on the proposed two strategies, as well as the compatibility and generalization ability. For simplicity, we refer to B²-DiffuRL as ours in this section.

4.1. Experimental Setup

Diffusion Models. Following the previous work [8], we use Stable Diffusion (SD) v1.4 as the backbone diffusion model, which has been widely used in academia and industry. We apply LoRA to UNet for efficient fine-tuning [26]. We employ DDIM [58] algorithm for sampling. Following



Figure 4. **(Samples)** Examples of images generated by different methods on three templates. For each set of images, we use the same random seed. Our method achieves better prompt-image alignment compared to vanilla Stable Diffusion and DDPO.

the previous work [8], we set the total denoising timesteps $T = 20$. The weight of noise is set to 1.0, which decides the degree of randomness of each denoising in DDIM. Each experiment is conducted with three different seeds.

Prompt Templates. In the sampling phase, we construct the prompts based on three different templates. The three prompt templates consider the behavior of the object, the attribute of the object, and the positional relationship between the objects in turn, which we believe can cover a wide range of commonly used prompts in image generation. (1) Template 1: “*a(n) [animal] [activity]*”. We use this template designed by DDPO. The animal is chosen from the list of 45 common animals, and randomly matched with an activity from the list: “*riding a bike*”, “*playing chess*” and “*washing dishes*”. (2) Template 2: “*[color] [fruit/vegetable]*”. This template focuses on object attributes. To construct a list of color-fruit/vegetable combinations, we query GPT-4 [1] about fruits/vegetables’ names and their common colors. We require each item to have at least 3 colors, and we end up building 40 prompts for this template. (3) Template 3: “*[object 1] [predicate] [object 2]*”. The predicates refer to positional relationship. We construct the prompts based on the annotations of Visual Relation Dataset [38]. We choose four predicates: “*on*”, “*under*”, “*on the left of*”, and “*on the right of*”, and end up with 40 prompts for this template. The prompts mentioned above are only used for training. In order to evaluate the generalization ability, we further construct prompts that will not be used in training. The full prompt lists are shown in the Appendix H.

Rewards. We score the prompt-image alignment by BERTScore and CLIPScore, and use them as reward functions: (1) BERTScore is introduced by DDPO [8], in which one uses the visual language model, such as LLaVA [36], to generate a description of the image, and then uses BERT’s

recall metric [14] to measure the semantic similarity between the prompt and the description. (2) CLIPScore is simply the similarity between text embedding and image embedding measured by CLIP model [7, 47]. We recommend using CLIPScore as reward function due to the instability of BERTScore, as shown in Appendix F.1. For implementations, we use 7b half-precision LLaVA v1.5 model [35], DeBERTa xlarge model [21] (a variant of BERT model), and ViT-H-14 CLIP model [47], respectively. To improve the stability of training, we normalize the rewards, as described in detail in Appendix D.1.

Evaluation Metrics. In this paper, we focus on both prompt-image alignment and image diversity. For alignment, we use BERTScore [8] and CLIPScore [7, 47] as metrics, the same as reward functions. A higher BERTScore or CLIPScore represents better prompt-image alignment. For diversity, following previous works [2, 4, 7, 74], we use inception score (IS) as the metric. A higher inception score represents better image diversity.

4.2. Qualitative Evaluation

We first evaluate the performance of our method and DDPO on the three prompt templates rewarded by CLIPScore. We use our method and DDPO respectively to fine-tune the diffusion model. After the same round of training, we sample some images from original model and fine-tuned models, as shown in Figure 4. The results qualitatively show that our method performs better than DDPO in improving the prompt-image alignment. We also conduct human preference test over 80 independent human raters (from undergrad to Ph.D.), who are asked to pick the best fit to prompt among three images generated by different models. As shown in Figure 7, the images generated by our method get higher preference rates than original SD and DDPO on all the three

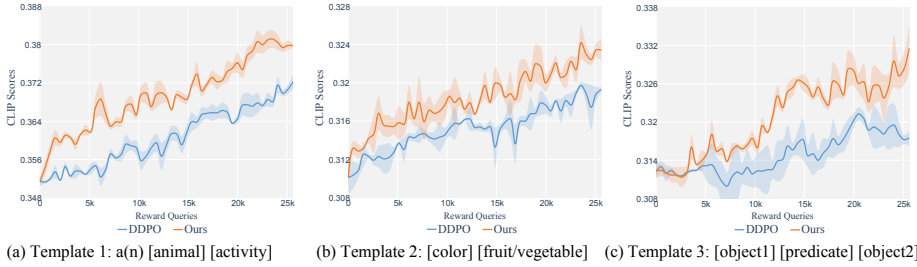


Figure 5. **(Alignment)** Alignment curves of our method and DDPO on three prompt templates.

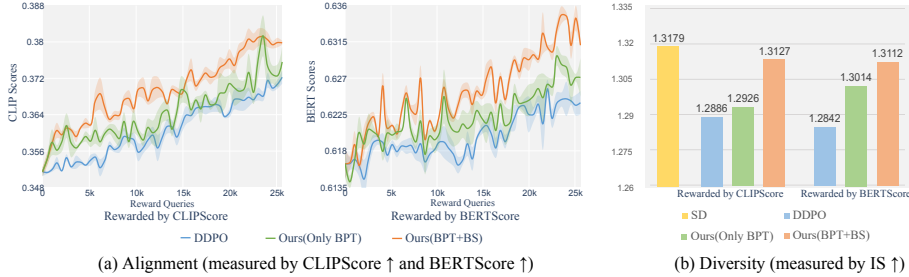


Figure 6. **(Ablation Study)** We separately evaluate the impact of each proposed strategy on prompt-image alignment and image diversity with template 1. (a) Both BPT and BS strategies help improve prompt-image alignment. (b) BS strategy also helps to maintain image diversity.

prompt templates. Also, images by our method are more diverse than those by DDPO. For example, on template 1, all images by DDPO adopt a cartoon style, while those by ours keep original styles of SD; on templates 2 and 3, backgrounds of the images by DDPO tend to reduce to a single color, while those by ours do not. This can be seen more clearly from Appendix G.

4.3. Quantitative Evaluation

We compare our method with DDPO quantitatively in terms of prompt-image alignment and diversity.

Prompt-Image Alignment. Figure 5 shows the curve of CLIPScore when fine-tuning the diffusion models using our method and DDPO as the amount of reward queries increases. We can observe that our method almost always achieves higher CLIPScore during fine-tuning on all the three prompts. This shows that our approach can improve prompt-image alignment better with the same number of reward queries compared to DDPO, which is due to our proposed two strategies.

Image Diversity. We evaluate the diversity of the images generated by original SD and the models fine-tuned by our method and DDPO. The results are shown in Table 1. After 25.6k reward queries during fine-tuning, both the models trained by ours and DDPO exhibit a reduction in diversity, since there is an inherent trade-off between alignment and diversity [72]. However, we find that the models trained

Methods	Temp. 1	Temp. 2	Temp. 3
SD	1.3179	1.4133	1.3582
DDPO	1.2886	1.3323	1.3273
Ours	1.3127	1.3579	1.3348

Table 1. **(Diversity)** IS ↑ of images generated by the SD [52], DDPO [8], and ours on three templates. There is a trade-off between alignment and diversity, while our method helps maintain diversity.

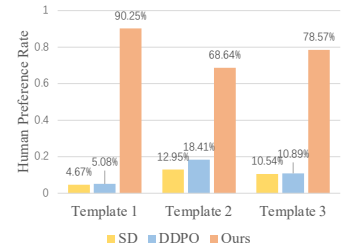


Figure 7. **(Human Evaluation)** Human preference rates for prompt-image alignment of images generated by SD, DDPO and our method.

by our method have a smaller reduction in diversity on all templates. For example, on template 1, the diversity of the model trained by our method decreases much less than that of DDPO, and is basically the same as the original model. Overall, our method can mitigate the reduction in image diversity during RL-based diffusion model fine-tuning.

4.4. Ablation Study

We separately evaluate the impact of each proposed strategy on alignment and diversity respectively.

Ablation Study on BPT Strategy. To evaluate the effectiveness of BPT, we fine-tune Stable Diffusion with only BPT strategy, rewarded by CLIPScore and BERTScore respectively. As shown in Figure 6 (a), regardless of the reward function, our proposed BPT strategy outperforms DDPO in terms of alignment. As we previously analyzed, BPT simplifies learning by training in stages, alleviating the negative effects of sparse rewards, and thus improving alignment. Moreover, since we only train models on timesteps of current training interval instead of all the denoising process, the computation costs of our method are less than DDPO for each queried reward.

Ablation Study on BS Strategy. The effectiveness of BS strategy on prompt-image alignment is shown in Figure 6 (a). We can observe that, based on BPT, the BS strategy further improves alignment in terms of both BERTScore and CLIPScore. By comparing contrastive

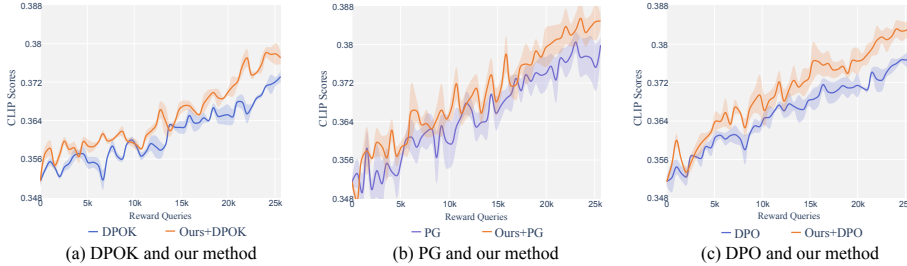


Figure 8. **(Compatibility: Alignment)** Alignment curves of our method on template 1 when compatible with difference RL algorithms.

Methods	Vanilla	Ours+Vanilla
SD	1.3179	-
DPOK	1.2785	1.3005
PG	1.2462	1.2896
DPO	1.2895	1.3051

Table 2. **(Compatibility: Diversity)** IS \uparrow of images on template 1 generated by our method when compatible with different RL algorithms.

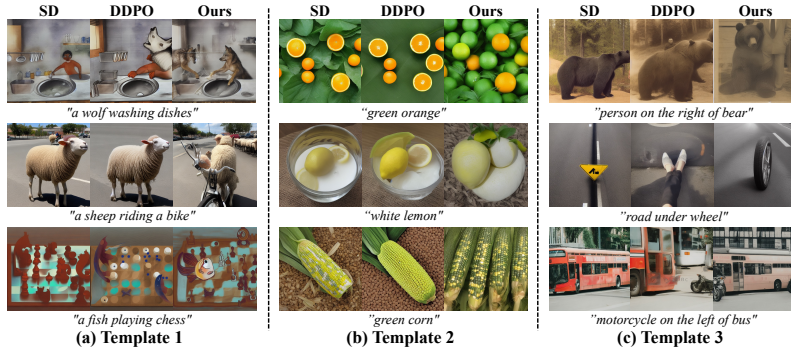


Figure 9. **(Generalization)** Examples of images generated by SD, DDPO and ours on three templates. The prompts are not used in training. We use the same seed for sampling.

Methods	Temp. 1	Temp. 2	Temp. 3
SD	0.3515	0.3168	0.2977
DDPO	0.3698	0.3175	0.3134
Ours	0.3748	0.3252	0.3183

Table 3. **(Generalization)** Prompt-image alignment (measured by CLIPScore \uparrow) of the generated images by SD, DDPO and our method on the prompts based on three templates. The prompts are not used during the training process.

samples, BS provides a clear indication of how much the policies of current training interval contribute to final images. This helps the model to learn effective policies. Additionally, as shown in Figure 6 (b), diversity of generated images always suffers from reduction since there is a trade-off between alignment and diversity. Fortunately, the BS strategy helps models avoid learning unnecessary policies, thereby contributing to maintaining image diversity. With BS strategy, diversity of the fine-tuned model decreases less, and even achieves similar diversity as the original SD.

4.5. Compatibility

Our framework B^2 -DiffuRL is compatible with various RL algorithms, not limited to DDPO. We further apply B^2 -DiffuRL to some widely used RL algorithms in diffusion model fine-tuning, including DPOK [17], policy gradient (PG) [57] and direct preference optimization (DPO) [48, 63]. The implementation details are shown in Appendix D.1. On the one hand, as we can see from Figure 8, when compatible with different RL algorithms, our method can help each of them to improve alignment to a greater extent. On the other hand, as shown in Table 2, while all algorithms reduce the diversity of generated images, our method can help mitigate the reduction. These experimental results further illustrate the effectiveness of our method in terms of both prompt-image alignment and diversity when applied to various RL algorithms.

4.6. Generalization Ability

Models fine-tuned by our method show generalization capabilities. We generate 1,600 images on the prompts based on the corresponding templates but not belong to the training lists, and test the prompt-image alignment on CLIPScore. As shown in Table 3, compared with DDPO, the models fine-tuned with our method also perform better on these prompts not used for training. Figure 9 shows examples of images generated on these prompts, qualitatively illustrating the good generalization ability of the models fine-tuned with our method. More samples can be seen in Appendix G.

5. Conclusions

In this work, we mitigated the issues of prompt-image misalignment in text-to-image diffusion models by reinforcement learning (RL). We highlight the challenge of sparse reward when training diffusion models with RL. By introducing a compatible RL-based fine-tuning framework B^2 -DiffuRL that leverages backward progressive training and branch-based sampling strategies, we effectively mitigated the negative effects of sparse reward. Using Stable Diffusion as backbone, we performed extensive experiments with various kinds of text prompts. Both qualitative and quantitative experimental results demonstrate that, compared with naive RL-based diffusion model training method, the proposed framework achieves better prompt-image alignment while sacrificing less image diversity.

References

- [1] Josh Achiam, Steven Adler, Sandhini Agarwal, Lama Ahmad, Ilge Akkaya, Florencia Leoni Aleman, Diogo Almeida, Janko Altenschmidt, Sam Altman, Shyamal Anadkat, et al. Gpt-4 technical report. *arXiv preprint arXiv:2303.08774*, 2023. 6
- [2] Sungsoo Ahn, Shell Xu Hu, Andreas Damianou, Neil D. Lawrence, and Zhenwen Dai. Variational information distillation for knowledge transfer, 2019. 6, 17
- [3] Marcin Andrychowicz, Filip Wolski, Alex Ray, Jonas Schneider, Rachel Fong, Peter Welinder, Bob McGrew, Josh Tobin, OpenAI Pieter Abbeel, and Wojciech Zaremba. Hindsight experience replay. *Advances in neural information processing systems*, 30, 2017. 3
- [4] Shane Barratt and Rishi Sharma. A note on the inception score, 2018. 6, 17
- [5] Georgios Batzolis, Jan Stanczuk, Carola-Bibiane Schönlieb, and Christian Etmann. Conditional image generation with score-based diffusion models. *arXiv preprint arXiv:2111.13606*, 2021. 3
- [6] James Betker, Gabriel Goh, Li Jing, Tim Brooks, Jianfeng Wang, Linjie Li, Long Ouyang, Juntang Zhuang, Joyce Lee, Yufei Guo, et al. Improving image generation with better captions. *Computer Science*. <https://cdn.openai.com/papers/dall-e-3.pdf>, 2(3):8, 2023. 1
- [7] Fengxiang Bie, Yibo Yang, Zhongzhu Zhou, Adam Ghanem, Minjia Zhang, Zhewei Yao, Xiaoxia Wu, Connor Holmes, Pareesa Golnari, David A. Clifton, Yuxiong He, Dacheng Tao, and Shuaiwen Leon Song. Renaissance: A survey into ai text-to-image generation in the era of large model, 2023. 6, 17
- [8] Kevin Black, Michael Janner, Yilun Du, Ilya Kostrikov, and Sergey Levine. Training diffusion models with reinforcement learning. 2023. 1, 2, 3, 4, 5, 6, 7, 17
- [9] Paul F Christiano, Jan Leike, Tom Brown, Miljan Martic, Shane Legg, and Dario Amodei. Deep reinforcement learning from human preferences. *Advances in neural information processing systems*, 30, 2017. 3
- [10] Kevin Clark, Paul Vicol, Kevin Swersky, and David J Fleet. Directly fine-tuning diffusion models on differentiable rewards, 2024. 3
- [11] Antonio Coronato, Muddasar Naeem, Giuseppe De Pietro, and Giovanni Paragliola. Reinforcement learning for intelligent healthcare applications: A survey. *Artificial Intelligence in Medicine*, 109:101964, 2020. 3
- [12] Jia Deng, Wei Dong, Richard Socher, Li-Jia Li, Kai Li, and Li Fei-Fei. Imagenet: A large-scale hierarchical image database. In *2009 IEEE Conference on Computer Vision and Pattern Recognition*, pages 248–255, 2009. 17
- [13] Rati Devidze, Parameswaran Kamalaruban, and Adish Singla. Exploration-guided reward shaping for reinforcement learning under sparse rewards. *Advances in Neural Information Processing Systems*, 35:5829–5842, 2022. 2, 3
- [14] Jacob Devlin, Ming-Wei Chang, Kenton Lee, and Kristina Toutanova. Bert: Pre-training of deep bidirectional transformers for language understanding. *arXiv preprint arXiv:1810.04805*, 2018. 6
- [15] Prafulla Dhariwal and Alexander Quinn Nichol. Diffusion models beat GANs on image synthesis. In *Advances in Neural Information Processing Systems*, 2021. 1, 3
- [16] Dave Epstein, Allan Jabri, Ben Poole, Alexei Efros, and Aleksander Holynski. Diffusion self-guidance for controllable image generation. *Advances in Neural Information Processing Systems*, 36:16222–16239, 2023. 3
- [17] Ying Fan, Olivia Watkins, Yuqing Du, Hao Liu, Moonkyung Ryu, Craig Boutilier, Pieter Abbeel, Mohammad Ghavamzadeh, Kangwook Lee, and Kimin Lee. Dpok: Reinforcement learning for fine-tuning text-to-image diffusion models. *arXiv preprint arXiv:2305.16381*, 2023. 1, 3, 4, 8, 14
- [18] Ian Goodfellow, Jean Pouget-Abadie, Mehdi Mirza, Bing Xu, David Warde-Farley, Sherjil Ozair, Aaron Courville, and Yoshua Bengio. Generative adversarial networks. *Communications of the ACM*, 63(11):139–144, 2020. 3, 17
- [19] Abhishek Gupta, Aldo Pacchiano, Yuexiang Zhai, Sham Kakade, and Sergey Levine. Unpacking reward shaping: Understanding the benefits of reward engineering on sample complexity. *Advances in Neural Information Processing Systems*, 35:15281–15295, 2022. 2, 3
- [20] Joshua Hare. Dealing with sparse rewards in reinforcement learning. *arXiv preprint arXiv:1910.09281*, 2019. 2, 3
- [21] Pengcheng He, Xiaodong Liu, Jianfeng Gao, and Weizhu Chen. Deberta: Decoding-enhanced bert with disentangled attention. In *International Conference on Learning Representations*, 2021. 6
- [22] Jonathan Ho and Tim Salimans. Classifier-free diffusion guidance. In *NeurIPS 2021 Workshop on Deep Generative Models and Downstream Applications*, 2021. 3
- [23] Jonathan Ho, Ajay Jain, and Pieter Abbeel. Denoising diffusion probabilistic models. In *Advances in Neural Information Processing Systems*, 2020. 1, 3, 4
- [24] Jonathan Ho, Chitwan Saharia, William Chan, David J Fleet, Mohammad Norouzi, and Tim Salimans. Cascaded diffusion models for high fidelity image generation. *Journal of Machine Learning Research*, 23(47):1–33, 2022. 3
- [25] Steven C. H. Hoi, Doyen Sahoo, Jing Lu, and Peilin Zhao. Online learning: A comprehensive survey, 2018. 2
- [26] Edward J. Hu, Yelong Shen, Phillip Wallis, Zeyuan Allen-Zhu, Yuanzhi Li, Shean Wang, Lu Wang, and Weizhu Chen. Lora: Low-rank adaptation of large language models, 2021. 3, 5
- [27] Yujing Hu, Weixun Wang, Hangtian Jia, Yixiang Wang, Yingfeng Chen, Jianye Hao, Feng Wu, and Changjie Fan. Learning to utilize shaping rewards: A new approach of reward shaping. *Advances in Neural Information Processing Systems*, 33:15931–15941, 2020. 2, 3
- [28] Dongzhi Jiang, Guanglu Song, Xiaoshi Wu, Renrui Zhang, Dazhong Shen, Zhuofan Zong, Yu Liu, and Hongsheng Li. Comat: Aligning text-to-image diffusion model with image-to-text concept matching. *arXiv preprint arXiv:2404.03653*, 2024. 1
- [29] Leslie Pack Kaelbling, Michael L Littman, and Andrew W Moore. Reinforcement learning: A survey. *Journal of artificial intelligence research*, 4:237–285, 1996. 1, 3

- [30] Sham Kakade and John Langford. Approximately optimal approximate reinforcement learning. In *Proceedings of the Nineteenth International Conference on Machine Learning*, pages 267–274, 2002. 5
- [31] Nupur Kumari, Bingliang Zhang, Richard Zhang, Eli Shechtman, and Jun-Yan Zhu. Multi-concept customization of text-to-image diffusion. In *Proceedings of the IEEE/CVF Conference on Computer Vision and Pattern Recognition*, pages 1931–1941, 2023. 3
- [32] Kimin Lee, Hao Liu, Moonkyung Ryu, Olivia Watkins, Yuqing Du, Craig Boutilier, Pieter Abbeel, Mohammad Ghavamzadeh, and Shixiang Shane Gu. Aligning text-to-image models using human feedback. *arXiv preprint arXiv:2302.12192*, 2023. 1, 3
- [33] Shufan Li, Konstantinos Kallidromitis, Akash Gokul, Yusuke Kato, and Kazuki Kozuka. Aligning diffusion models by optimizing human utility, 2024. 3
- [34] Xiang Li, John Thickstun, Ishaan Gulrajani, Percy S Liang, and Tatsunori B Hashimoto. Diffusion-lm improves controllable text generation. *Advances in Neural Information Processing Systems*, 35:4328–4343, 2022. 3
- [35] Haotian Liu, Chunyuan Li, Yuheng Li, and Yong Jae Lee. Improved baselines with visual instruction tuning. *arXiv preprint arXiv:2310.03744*, 2023. 6
- [36] Haotian Liu, Chunyuan Li, Qingyang Wu, and Yong Jae Lee. Visual instruction tuning. 2023. 6
- [37] Ilya Loshchilov and Frank Hutter. Decoupled weight decay regularization, 2019. 16
- [38] Cewu Lu, Ranjay Krishna, Michael Bernstein, and Li Fei-Fei. Visual relationship detection with language priors. In *European Conference on Computer Vision*, 2016. 6
- [39] Nguyen Cong Luong, Dinh Thai Hoang, Shimin Gong, Dusit Niyato, Ping Wang, Ying-Chang Liang, and Dong In Kim. Applications of deep reinforcement learning in communications and networking: A survey. *IEEE communications surveys & tutorials*, 21(4):3133–3174, 2019. 3
- [40] Farzan Memarian, Wonjoon Goo, Rudolf Lioutikov, Scott Niekum, and Ufuk Topcu. Self-supervised online reward shaping in sparse-reward environments. In *2021 IEEE/RSJ International Conference on Intelligent Robots and Systems (IROS)*, pages 2369–2375. IEEE, 2021. 2, 3
- [41] Shakir Mohamed, Mihaela Rosca, Michael Figurnov, and Andriy Mnih. Monte carlo gradient estimation in machine learning. *The Journal of Machine Learning Research*, 21(1): 5183–5244, 2020. 4
- [42] Ofir Nachum, Shixiang Shane Gu, Honglak Lee, and Sergey Levine. Data-efficient hierarchical reinforcement learning. *Advances in neural information processing systems*, 31, 2018. 3
- [43] Andrew Y Ng, Daishi Harada, and Stuart Russell. Policy invariance under reward transformations: Theory and application to reward shaping. In *Icml*, pages 278–287, 1999. 2, 3
- [44] Alexander Quinn Nichol and Prafulla Dhariwal. Improved denoising diffusion probabilistic models. In *International Conference on Machine Learning*, 2021. 3
- [45] Athanasios S Polydoros and Lazaros Nalpantidis. Survey of model-based reinforcement learning: Applications on robotics. *Journal of Intelligent & Robotic Systems*, 86(2): 153–173, 2017. 3
- [46] Mihir Prabhudesai, Anirudh Goyal, Deepak Pathak, and Katerina Fragkiadaki. Aligning text-to-image diffusion models with reward backpropagation. *arXiv preprint arXiv:2310.03739*, 2023. 1, 3
- [47] Alec Radford, Jong Wook Kim, Chris Hallacy, Aditya Ramesh, Gabriel Goh, Sandhini Agarwal, Girish Sastry, Amanda Askell, Pamela Mishkin, Jack Clark, Gretchen Krueger, and Ilya Sutskever. Learning transferable visual models from natural language supervision. *arXiv preprint arXiv:2103.00020*, 2021. 6
- [48] Rafael Rafailov, Archit Sharma, Eric Mitchell, Stefano Ermon, Christopher D. Manning, and Chelsea Finn. Direct preference optimization: Your language model is secretly a reward model, 2023. 3, 8
- [49] Aditya Ramesh, Mikhail Pavlov, Scott Gray Gabriel Goh, Chelsea Voss, Alec Radford, Mark Chen, and Ilya Sutskever. Zero-shot text-to-image generation. *arXiv preprint arXiv:2102.12092*, 2021. 1, 3
- [50] Martin Riedmiller, Roland Hafner, Thomas Lampe, Michael Neunert, Jonas Degraeve, Tom Wiele, Vlad Mnih, Nicolas Heess, and Jost Tobias Springenberg. Learning by playing solving sparse reward tasks from scratch. In *International conference on machine learning*, pages 4344–4353. PMLR, 2018. 2, 3
- [51] Robin Rombach, Andreas Blattmann, Dominik Lorenz, Patrick Esser, and Björn Ommer. High-resolution image synthesis with latent diffusion models, 2022. 3
- [52] Robin Rombach, Andreas Blattmann, Dominik Lorenz, Patrick Esser, and Björn Ommer. High-resolution image synthesis with latent diffusion models. In *IEEE Conference on Computer Vision and Pattern Recognition*, 2022. 1, 3, 4, 7
- [53] Nataniel Ruiz, Yuanzhen Li, Varun Jampani, Yael Pritch, Michael Rubinstein, and Kfir Aberman. Dreambooth: Fine tuning text-to-image diffusion models for subject-driven generation. In *Proceedings of the IEEE/CVF Conference on Computer Vision and Pattern Recognition*, pages 22500–22510, 2023. 3
- [54] Seyedmorteza Sadat, Jakob Buhmann, Derek Bradely, Otmar Hilliges, and Romann M Weber. Cads: Unleashing the diversity of diffusion models through condition-annealed sampling. *arXiv preprint arXiv:2310.17347*, 2023. 2
- [55] Chitwan Saharia, William Chan, Saurabh Saxena, Lala Li, Jay Whang, Emily Denton, Seyed Kamyar Seyed Ghasemipour, Burcu Karagol Ayan, S. Sara Mahdavi, Rapha Gontijo Lopes, Tim Salimans, Jonathan Ho, David J Fleet, and Mohammad Norouzi. Photorealistic text-to-image diffusion models with deep language understanding. *arXiv preprint arXiv:2205.11487*, 2022. 3
- [56] Chitwan Saharia, William Chan, Saurabh Saxena, Lala Li, Jay Whang, Emily L Denton, Kamyar Ghasemipour, Raphael Gontijo Lopes, Burcu Karagol Ayan, Tim Salimans, et al. Photorealistic text-to-image diffusion models with deep language understanding. *Advances in neural information processing systems*, 35:36479–36494, 2022. 1

- [57] John Schulman, Filip Wolski, Prafulla Dhariwal, Alec Radford, and Oleg Klimov. Proximal policy optimization algorithms. *arXiv preprint arXiv:1707.06347*, 2017. 3, 5, 8, 12
- [58] Jiaming Song, Chenlin Meng, and Stefano Ermon. Denoising diffusion implicit models, 2022. 4, 5
- [59] Yang Song and Stefano Ermon. Improved techniques for training score-based generative models. In *Advances in neural information processing systems*, 2020. 1, 3
- [60] Fareena Sultan, John U Farley, and Donald R Lehmann. A meta-analysis of applications of diffusion models. *Journal of marketing research*, 27(1):70–77, 1990. 3
- [61] Christian Szegedy, Vincent Vanhoucke, Sergey Ioffe, Jonathon Shlens, and Zbigniew Wojna. Rethinking the inception architecture for computer vision, 2015. 17
- [62] Alexander Trott, Stephan Zheng, Caiming Xiong, and Richard Socher. Keeping your distance: Solving sparse reward tasks using self-balancing shaped rewards. *Advances in Neural Information Processing Systems*, 32, 2019. 2, 3
- [63] Bram Wallace, Meihua Dang, Rafael Rafailov, Linqi Zhou, Aaron Lou, Senthil Purushwalkam, Stefano Ermon, Caiming Xiong, Shafiq Joty, and Nikhil Naik. Diffusion model alignment using direct preference optimization, 2023. 1, 3, 4, 8
- [64] Zhendong Wang, Yifan Jiang, Huangjie Zheng, Peihao Wang, Pengcheng He, Zhangyang Wang, Weizhu Chen, Mingyuan Zhou, et al. Patch diffusion: Faster and more data-efficient training of diffusion models. *Advances in Neural Information Processing Systems*, 36, 2024. 1
- [65] Jiazheng Xu, Xiao Liu, Yuchen Wu, Yuxuan Tong, Qinkai Li, Ming Ding, Jie Tang, and Yuxiao Dong. Imagereward: Learning and evaluating human preferences for text-to-image generation. *arXiv preprint arXiv:2304.05977*, 2023. 1, 3
- [66] Kai Yang, Jian Tao, Jiafei Lyu, Chunjiang Ge, Jiabin Chen, Weihao Shen, Xiaolong Zhu, and Xiu Li. Using human feedback to fine-tune diffusion models without any reward model. In *Proceedings of the IEEE/CVF Conference on Computer Vision and Pattern Recognition (CVPR)*, pages 8941–8951, 2024. 3
- [67] Ling Yang, Zhilong Zhang, Yang Song, Shenda Hong, Runsheng Xu, Yue Zhao, Wentao Zhang, Bin Cui, and Ming-Hsuan Yang. Diffusion models: A comprehensive survey of methods and applications. *ACM Computing Surveys*, 56(4): 1–39, 2023. 3
- [68] Shentao Yang, Tianqi Chen, and Mingyuan Zhou. A dense reward view on aligning text-to-image diffusion with preference. In *Forty-first International Conference on Machine Learning*, 2024. 3
- [69] Zhongqi Yue, Jiankun Wang, Qianru Sun, Lei Ji, Eric I Chang, Hanwang Zhang, et al. Exploring diffusion time-steps for unsupervised representation learning. *arXiv preprint arXiv:2401.11430*, 2024. 2
- [70] Zhongqi Yue, Pan Zhou, Richang Hong, Hanwang Zhang, and Qianru Sun. Few-shot learner parameterization by diffusion time-steps. *arXiv preprint arXiv:2403.02649*, 2024. 2
- [71] Chenshuang Zhang, Chaoning Zhang, Mengchun Zhang, and In So Kweon. Text-to-image diffusion model in generative ai: A survey. *arXiv preprint arXiv:2303.07909*, 2023. 3
- [72] Guanhua Zhang and Moritz Hardt. Inherent trade-offs between diversity and stability in multi-task benchmark. *arXiv preprint arXiv:2405.01719*, 2024. 2, 7
- [73] Lvmin Zhang, Anyi Rao, and Maneesh Agrawala. Adding conditional control to text-to-image diffusion models. In *Proceedings of the IEEE/CVF International Conference on Computer Vision*, pages 3836–3847, 2023. 3
- [74] Shengyu Zhao, Zhijian Liu, Ji Lin, Jun-Yan Zhu, and Song Han. Differentiable augmentation for data-efficient gan training. In *Conference on Neural Information Processing Systems (NeurIPS)*, 2020. 6, 17

The **Appendix** is organized as follows:

- **Appendix A:** discusses the potential broader impacts of our work.
- **Appendix B:** gives the list of abbreviations and symbols in our paper.
- **Appendix C:** gives a comprehensive discussion on the challenge of sparse reward.
- **Appendix D:** provides more details on implementation (e.g., experimental resources and hyperparameters).
- **Appendix E:** provides pseudo-code of B²-DiffuRL.
- **Appendix F:** gives an discussion on evaluation metrics, including comparison between BERTScore and CLIP-Score, and inception score.
- **Appendix G:** provides more image samples generated by the diffusion models fine-tuned with B²-DiffuRL.
- **Appendix H:** provides the prompt lists used in our experiments.

A. Broader Impacts

Generative models, particularly diffusion models, are powerful productivity tools with significant potential for positive applications. However, their misuse can lead to undesirable consequences. Our research focuses on improving the prompt-image alignment of diffusion models, enhancing their accuracy and usefulness in fields such as medical image synthesis. While these advancements have clear benefits, they also pose risks, including the creation of false information that can mislead the public and manipulate public opinion. Therefore, ensuring reliable detection of synthesized content is crucial to mitigate the potential harm associated with generative models.

B. Abbreviation and Symbol Table

The list of important abbreviations and symbols in this paper goes as Table 4.

C. A Comprehensive Discussion on Sparse Rewards

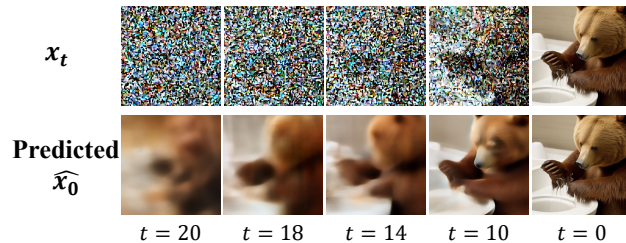


Figure 10. (**Examples for Predicted \hat{x}_0**) This figure shows the x_t and predicted \hat{x}_0 in the denoising process.

(1) How does the sparse reward make a negative impact on RL-based diffusion models fine-tuning? The reward is sparse when we execute RL-based diffusion models fine-tuning, since only the final image x_0 is available to evaluate

the text-image alignment. Previous works such as DDPO and DPOK have to treat the denoising actions at different timesteps equally and set $r_{T-1} = r_{T-2} = \dots = r_0$. However, we argue that the denoising actions a_t on different timesteps have different effects on alignment, and the unreasonable reward setting is not conducive to learning. For example, as shown in Figure 11, the images x_0^1 , x_0^2 , and x_0^3 have the same parent node x_{14}^1 but different text-image alignment scores. The reason for their difference is that different denoising actions $a_{13:1}$ (instead of $a_{20:14}$). Therefore, it is inappropriate to use sparse reward r_0 to reward denoising actions $a_{20:14}$. Besides, as shown in Table 5, the differences in alignment results under the same branch are common, even with a small number of timesteps $T = 20$. This reveals the universality of the sparse reward problem.

(2) Why not directly calculate the alignment score of the predicted \hat{x}_0 at each timestep t ? Each DDPM or DDIM denoising step can generate a corresponding predicted \hat{x}_0 using x_t and the predicted ϵ . However, as shown in Figure 10, the predicted \hat{x}_0 at most denoising steps is unclear. We do not think that the reward function for final images can make an accurate evaluation of intermediate images.

(3) How do the proposed BPT and BS strategies help to mitigate the sparse reward issue? BPT allows diffusion models to focus on specific training intervals (from τ to 0) rather than all timesteps (from T to 0). As training progresses, $a_{\tau:1}$ turn to align better, thus the alignment is more determined by $a_{T:\tau+1}$, and the final reward is more accurate for $a_{T:\tau+1}$. That is, BPT helps to assign more appropriate rewards to denoising actions $a_{T:\tau+1}$. BS samples different images from the same parent node x_τ and selects the best one and the worst one to form a contrastive sample pair. By comparing the contrastive sample pair, BS can provide more accurate rewards for denoising actions $a_{\tau:1}$, since the images within the same branch have the same state s_τ . Moreover, since the contrastive samples share high-level visual semantics such as image style, the models do not learn to generate images with a specific style. This is why our proposed strategies preserve higher diversity compared to naive RL algorithms.

D. Implementation Details

D.1. Implementation of Our Method

Proximal Policy Optimization. Following DDPO, we apply proximal policy optimization (PPO) algorithm [57], a commonly used family of policy gradient (PG) algorithm for reinforcement learning. And we perform importance sampling $\frac{p_\theta(x_{t-1}|x_t,c)}{p_{\theta_{old}}(x_{t-1}|x_t,c)}$ and clipping [57] to implement PPO.

Extendence of Training Interval. When employing backward progressive training, the training interval will extend gradually to cover all timesteps of the denoising process. In

Abbreviation/Symbol	Meaning
<i>Abbreviations of Concepts</i>	
DM	Diffusion Model
RL	Reinforcement Learning
SD	Stable Diffusion
LoRA	Low-Rank Adaptation
DDIM	Denosing Diffusion Implicit Model
CLIP	Contrastive Language-Image Pre-Training
BERT	Bidirectional Encoder Representation from Transformers
IS	Inception Score
<i>Abbreviations of Approaches</i>	
B ² -DiffuRL	BPT and BS for Reinforcement Learning in Diffusion models
BPT	Backward Progressive Training
BS	Branch-based Sampling
DDPO	Denosing Diffusion Policy Optimization
DPOK	Diffusion Policy Optimization with KL regularization
PG	Policy Gradient algorithm
DPO	Direct Preference Optimization
<i>Symbols of Diffusion Models</i>	
x_0	Generated image
x_t	Image with noise at timestep t
c	Condition for image generation, also called prompt
θ	Parameters of the diffusion model
$\mu_\theta, \Sigma_\theta$	Mean and variance predicted by the diffusion model
$\mathcal{N}()$	Gaussian distribution
T	Total timesteps
$[\tau, 1]$	Training interval from timestep τ to 1
<i>Symbols of Reinforcement Learning</i>	
s_t	State at timestep t
a_t	Action at timestep t
π_θ	Action selection policy parameterized by θ
$r()$	Reward function
$\hat{r}()$	Reward function with normalization

Table 4. List of important abbreviations and symbols.

practice, we use a linear expansion strategy. That is, given the initial training interval $[\tau_0, 1]$, the total timesteps T and total number of training round N , the training interval in round n is $[\tau_0 + \lfloor \frac{T-\tau_0+1}{N} \rfloor, 1]$.

Reward Normalization. The prompt-image alignment scores given by CLIP or BERT need to be normalized before being used as rewards in training. In practice, we compute the mean and variance of the scores for each training round, with the images generated by the same prompt in the current round and in the past several rounds. Then the score can be normalized as $\frac{\text{score}-\text{mean}}{\text{variance}}$. When computing mean and variance, we incorporate images from the past rounds into calculation, because calculation using only images from one single round may be inaccurate. However,

we only use images from the past few rounds, instead of all rounds, in the consideration that the scores of images multiple rounds ago differ greatly from those in current round as fine-tuning progresses, and are not suitable for estimating mean and variance of current round. In practice, we use images from the past 8 training rounds.

Compatibility with Policy Gradient. When applying PG, the value function $V(x_\tau, c)$ should be considered. In our implementation, we replace value function with the reward normalization mentioned above. What’s more, the importance sampling $\frac{p_\theta(x_{t-1}|x_t, c)}{p_{old}(x_{t-1}|x_t, c)}$ is also applied to improve stability of training. Therefore, the optimization objective of PG in our setting is the same as Eq. (6), but without using the clipping in PPO.

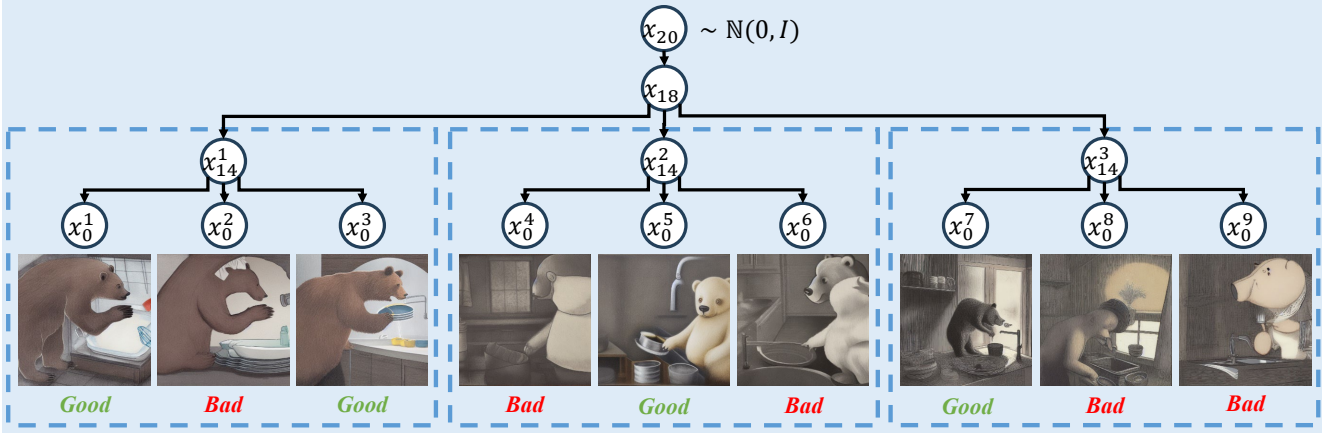


Figure 11. **(Examples Showing the Problem of Sparse Reward)** For these examples, the number of denoising timesteps T is set to 20, and the prompt is “a bear washing dishes”. The images are denoised from the same x_{18} with different seeds, and every 3 images are denoised from the same x_{14} with different seeds. As we can see, the images denoised from the same parent node x_{18} or x_{14} can get different alignment scores. We can not tell whether x_{18}/x_{14} is good or bad from one final image. Consequently, it is inappropriate to use the reward for the last timesteps as the reward for the whole denoising process.

Timestep when Branching	2	4	6	8	10	12	14	16	18	20
Proportion	8.2%	16.8%	15.6%	28.1%	28.9%	34.0%	43.0%	44.5%	52.3%	66.4%

Table 5. **(Proportion of branches that contain both well-aligned and poorly-aligned images when branching from different timesteps)** The number of denoising timesteps T is set to 20. We sample 256 branches each time, and each branch contains 3 images. The differences in alignment results under the same branch are widespread.

Compatibility with DPOK. DPOK also uses value function and clipping in their implementation. Same with PG, we replace value function with reward normalization. Therefore, the gradient of our method when compatible with DPOK goes as Eq. (7).

$$\mathbb{E} \left(\sum_{t=1}^{\tau} \left[-\alpha \nabla_{\theta} \log p_{\theta}(\mathbf{x}_{t-1}^{+} | \mathbf{x}_t^{+}, \mathbf{c}) \hat{r}^{+} + \beta \nabla_{\theta} \text{KL}(p_{\theta}(\mathbf{x}_{t-1}^{+} | \mathbf{x}_t^{+}, \mathbf{c}) || p_{\theta_{\text{old}}}(\mathbf{x}_{t-1}^{+} | \mathbf{x}_t^{+}, \mathbf{c})) - \alpha \nabla_{\theta} \log p_{\theta}(\mathbf{x}_{t-1}^{-} | \mathbf{x}_t^{-}, \mathbf{c}) \hat{r}^{-} + \beta \nabla_{\theta} \text{KL}(p_{\theta}(\mathbf{x}_{t-1}^{-} | \mathbf{x}_t^{-}, \mathbf{c}) || p_{\theta_{\text{old}}}(\mathbf{x}_{t-1}^{-} | \mathbf{x}_t^{-}, \mathbf{c})) \right] \right). \quad (7)$$

Compatibility with Direct Preference Optimization. In contrastive sample pairs, the positive samples are more preferred than negative samples. Therefore, we can apply direct preference optimization (DPO). The gradient of our method when compatible with DPO goes as Eq. (8).

$$-\mathbb{E} \left(\sum_{t=1}^{\tau} \left[\frac{p_{\theta}(\mathbf{x}_{t-1}^{+} | \mathbf{x}_t^{+}, \mathbf{c})}{p_{\theta_{\text{old}}}(\mathbf{x}_{t-1}^{+} | \mathbf{x}_t^{+}, \mathbf{c})} \nabla_{\theta} \log p_{\theta}(\mathbf{x}_{t-1}^{+} | \mathbf{x}_t^{+}, \mathbf{c}) - \frac{p_{\theta}(\mathbf{x}_{t-1}^{-} | \mathbf{x}_t^{-}, \mathbf{c})}{p_{\theta_{\text{old}}}(\mathbf{x}_{t-1}^{-} | \mathbf{x}_t^{-}, \mathbf{c})} \nabla_{\theta} \log p_{\theta}(\mathbf{x}_{t-1}^{-} | \mathbf{x}_t^{-}, \mathbf{c}) \right] \right). \quad (8)$$

D.2. Discussion on Value Function

A value function $V(x_t, c)$ is usually used in policy gradient training. By subtracting $r(x_0, c)$ with $V(x_t, c)$, the variance of gradient estimation can be minimized [17]. However, we do not employ value function in our implementation.

Branch-based sampling and reward normalization have the same effect as value function. Since value function is trained to minimize $E_{p_{\theta}(x_{0:t})} (r(x_0, c) - V(x_t, c))^2$, the state value $V(x_t, c)$ approximately equals to the mean score of the x_0 s denoised from the given x_t . In our approach, reward normalization, as detailed in Appendix D.1, normalizes the score/reward using $\frac{\text{score} - \text{mean}}{\text{variance}}$, similar to the effect of applying value function (i.e., $(r(x_0, c) - V(x_t, c))$). Simultaneously, branch-based sampling provides additional samples denoised from the given x_t , which improves the estimation of the mean score. Moreover, the contrastive samples are denoised from the same x_t , with differences in their rewards reflecting variations in the denoising process from x_t to x_0 . By constructing pair-wise contrastive samples, branch-based sampling (BS) introduces reward signals that are independent of previous timesteps, helping to estimate the reward of x_t accurately. This is also why applying BPT+BS consistently outperforms only applying BPT in our experiments.

Algorithm 1: Pseudo-code of B²-DiffuRL for one training round.

Input : Denoising timesteps T , inner epoch E , number of samples each round N , prompt list C , number of branches K , training interval $[\tau, 1]$, reward function r , pretrained diffusion model p_θ

```

.
pold = deepcopy(pθ) ;
pold.require_grad(False) ;
// Sampling
Dsampling = {} ;
for n ← 1 to N do
    Randomly choose a prompt c from C ;
    Randomly choose xT from N(0, I) ;
    x(T-1):τ = Denoise with pθ for (T - τ) steps ;
    for k ← 1 to K do
        xτk = deepcopy(xτ) ;
        x(τ-1):0k = Denoise with pθ for τ steps ;
    end
    Dsampling.push([xτ:01:K, c]) ;
end
// Evaluation
Dtraining = {} ;
for [xτ:01:K, c] ∈ Dsampling do
    s1:K = normalization(r(x01:K, c)) // Do normalization as Appendix D.1
    if s1:K contains both negative and positive scores then
        i = argmax(s1:K); j = argmin(s1:K);
        Dtraining.push([xti, xt-1i, si, xtj, xt-1j, sj, c]t=1:τ) // Contrastive sample pairs
    else
        i = argmax(abs(s1:K));
        Dtraining.push([xti, xt-1i, si, c]t=1:τ) // Simple samples
    end
end
// Training
for e ← 1 to E do
    D = shuffle(Dtraining) ;
    with grad ;
    for d ∈ D do
        d = shuffle(d) ;
        if d is a contrastive sample pair then
            for [xti, xt-1i, si, xtj, xt-1j, sj, c] ∈ d do
                | update θ with gradient descent using Eq. (6) ;
            end
        else
            for [xti, xt-1i, si, c] ∈ d do
                | update θ with gradient descent using Eq. (4) ;
            end
        end
    end
end

```

D.3. Computational Cost

In experiments, it takes about 36 hours to reach 50 epochs using B²-DiffuRL, while DDPO takes about 60 hours. Computational cost mainly consists of two parts: sampling and training. In training, for a sample x_0 , the vanilla training using RL algorithm needs to traverse the entire denoising process from x_T to x_0 , while the training using BPT only needs to traverse from x_τ to x_0 , where $\tau \leq T$. Therefore, using BPT leads to lower training cost in training. As for sampling, using branch-based sampling (BS) indeed leads to higher computational cost. However, sampling is much faster than training, so B²-DiffuRL requires lower computational cost overall.

D.4. Experimental Resources

We conducted experiments on 8 24GB NVIDIA 3090 GPUs. It took approximately 36 hours to reach 25.6k reward queries when rewarded by CLIPScore, and approximately 80 hours when rewarded by BERTScore (LLaVA inference would take much time).

D.5. Hyperparameters

We list hyperparameters of our experiments in Table 6.

	Hyperparameter	B ² -DiffuRL	DDPO
Sampling	Denosing steps T	20	20
	Noise Weight η	1.0	1.0
	Guidance Scale	5.0	5.0
	Batch size	8	8
	Batch count	32	32
	Number of Branches	3	-
Optimizer	Optimizer	AdamW [37]	AdamW
	Learning rate	1e-4	1e-4
	Weight decay	1e-4	1e-4
	(β_1, β_2)	(0.9, 0.999)	(0.9, 0.999)
	ϵ	1e-8	1e-8
Training	Batch size	2	2
	Grad. accum. steps	32	128
	Initial training interval	[14, 1]	-
	Score threshold	0.5	-

Table 6. Hyperparameters of our experiments.

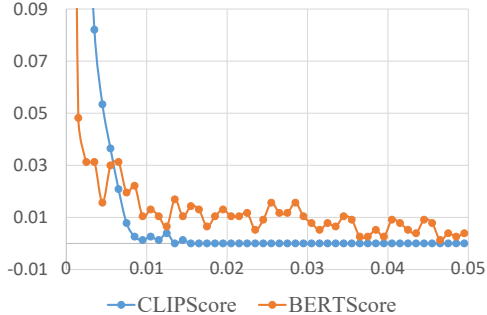
E. Pseudo-code

The pseudo-code of B²-DiffuRL for one training round goes as Algorithm 1.

F. Discussion on Evaluation Metrics

F.1. Comparison between BERTScore and CLIPScore

We create a dataset containing 768 pairs of similar images generated by diffusion models with 20 denoising steps. The



(a) Distribution of score differences for similar image pairs.



(b) Examples of similar image pairs.

Figure 12. (a) Distribution curve of score differences for similar image pairs when evaluated by CLIPScore and BERTScore. (b) Examples of similar image pairs.

two images in the same pair share the same states in the first 19 denoising steps, and only differ in the last denoising step. Some examples are shown in Figure 12 (b), and we can't tell the difference between them with our eyes. But they are different images, since their file size in JPEG format are different. Since images in same pairs are visually indistinguishable, they should receive similar prompt-image alignment scores.

However, BERTScores of similar image pairs differ a lot in our observation. Figure 12 (a) shows the distribution curves of score differences for similar image pairs, evaluated on CLIPScore and BERTScore. For CLIPScore, we can observe that almost all similar images have a score difference of less than 0.01. But for BERTScore, in the interval where the score difference is greater than 0.01, there are still many similar image pairs. As we can see from Figure 6 (a), after fine-tuning the model, BERTScores of the generated images increase by 0.01-0.03. In consideration of accurate rewarding and evaluation, it is intolerable that the score difference of similar images is greater than 0.01. Therefore, we recommend using CLIPScore as reward function instead of BERTScore.

F.2. Introduction to Inception Score

Following previous works [2, 4, 7, 74], we use inception score (IS) as the metric of image diversity. Inception score is primarily applied as an evaluation metric for GANs [18]. It uses a pretrained inception v3 model [61] to predict the conditional label distribution $P(y | x)$. Then the inception score is calculated as detailed in Eq. (9):

$$IS = \exp(\mathbb{E}_x(KL(p(y | x)||P(y))))), \quad (9)$$

where KL is Kullback-Leibler divergence. Traditional Inception v3 is trained only on ImageNet [12], while Stable Diffusion is trained on a large-scale dataset. In real implementation, in order to better measure the diversity of images, we replace it by the image encoder of CLIP for calculating IS. A higher inception score represents better image diversity.

G. More Samples

In this section, we show more samples generated by the diffusion models fine-tuned with our method B²-DiffuRL. Figure 13 shows more samples generated by our method compared with DDPO, DPO, PG and DPO on templeta 1. Figure 14 and 15 show more samples from our method on template 2 and 3 respectively. Figure 16 shows more samples of generalization to unseen prompts.

In Figure 17, more samples are generated on three given prompts to show the diversity of different methods. As we can see, most images generated by DDPO adopt a cartoon-like style, as described in their paper [8]. Especially for the images generated on the prompt “*a fox riding a bike*”, almost all the background information is lost and becomes a single color. On the contrary, the images generated by our method can almost keep the same style as SD, mitigating the problem of diversity reduction.



Figure 13. More samples generated by our method compared with other methods on template 1.

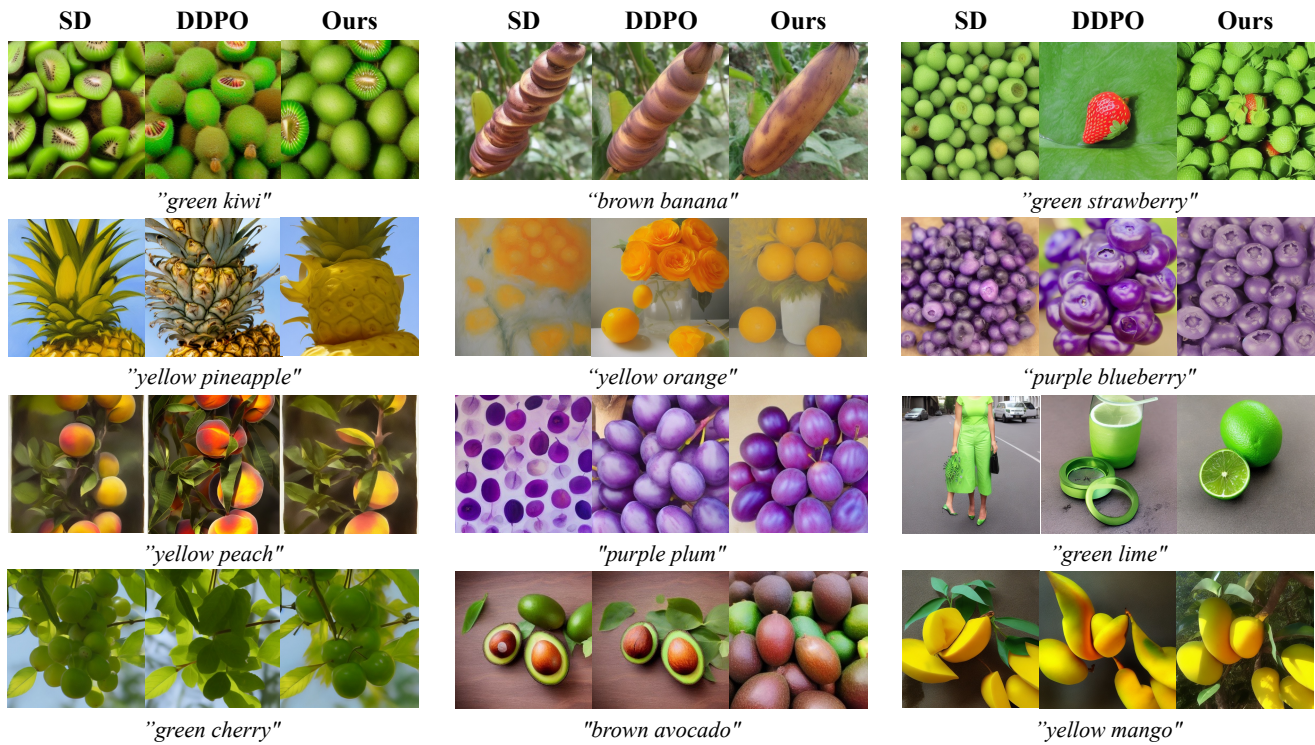


Figure 14. More samples generated by our method on template 2.

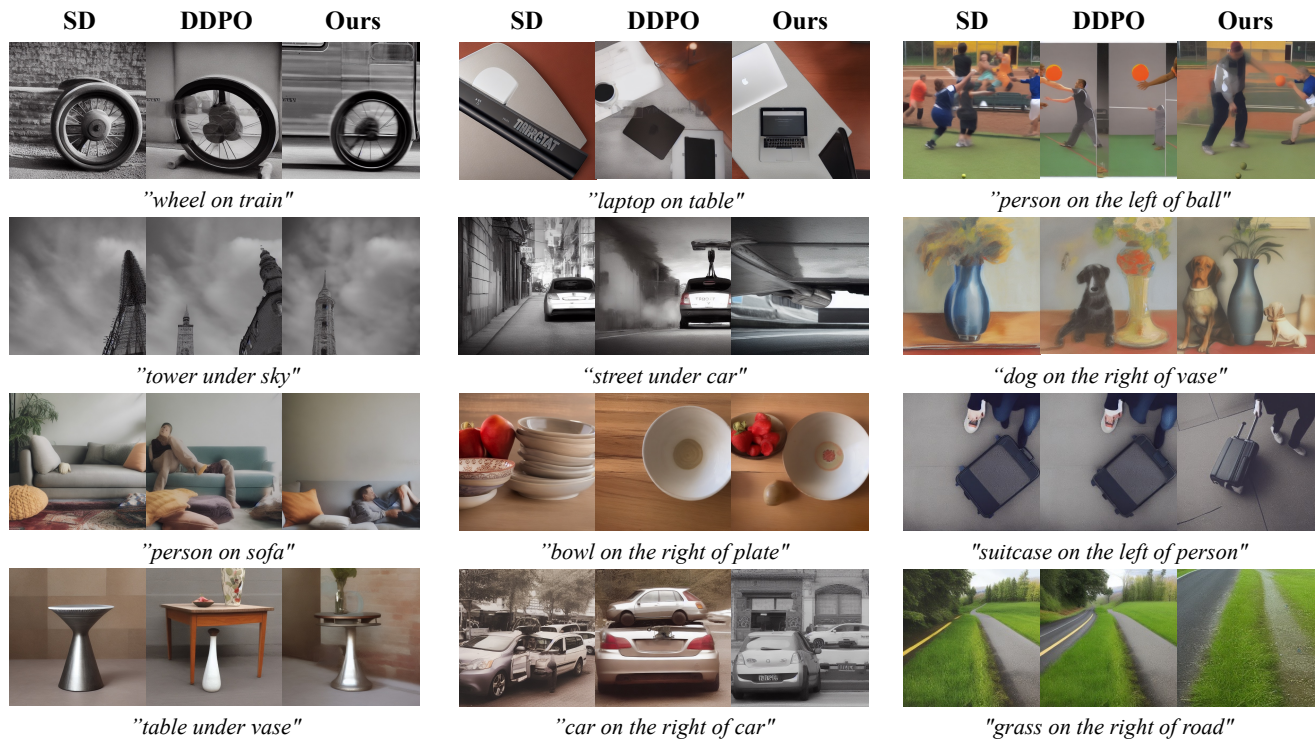


Figure 15. More samples generated by our method on template 3.



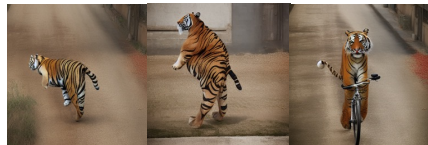
"a fox washing dishes"



"a butterfly playing chess"



"a chicken riding a bike"



"a tiger riding a bike"



"a lizard washing dishes"



"a whale playing chess"



"a snake playing chess"



"a pig riding a bike"

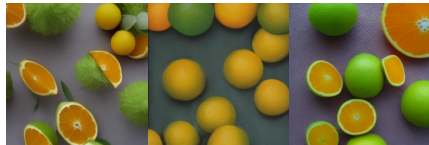
(a) Template 1



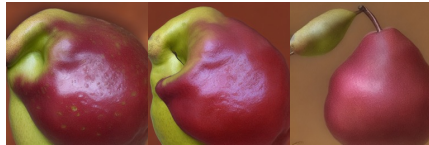
"green pineapple"



"white pomegranate"



"green orange"



"brown pear"



"red plum"



"red lettuce"



"white cabbage"



"green banana"

(b) Template 2



"watch on person"



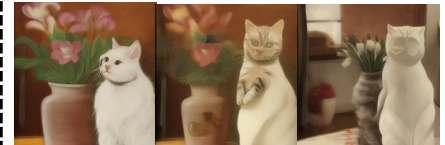
"person behind person"



"hydrant behind motorcycle"



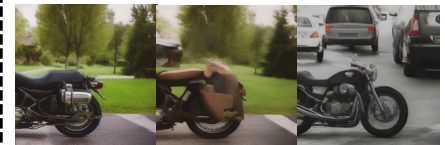
"road under wheel"



"cat in the front of vase"



"road under bus"



"motorcycle on the left of car"



"motorcycle behind person"

(c) Template 3

Figure 16. More samples of generalization to unseen prompts in template 1, 2 and 3.



"a fox riding a bike"



"a bear washing dishes"



"a pig playing chess"

Figure 17. More samples generated by SD, DDPO and our method on three prompts. The images generated by DDPO tend to adopt a cartoon style, while those by our method tend to keep original styles of SD. These samples show that our method can help mitigating the image diversity reduction during fine-tuning.

H. Prompt Lists

In this section, we provide the prompt lists used in our experiments. For each template, we collect one prompt list for training, and the other one for generalization test, as shown in Table 7, 8 and 9.

Training list		
a cat washing dishes a monkey washing dishes a spider washing dishes a deer washing dishes a lion washing dishes a raccoon riding a bike a lizard riding a bike a butterfly riding a bike a whale riding a bike a mouse riding a bike a turtle playing chess a duck playing chess a pig playing chess a llama playing chess a gorilla playing chess	a dog washing dishes a rabbit washing dishes a bird washing dishes a cow washing dishes a tiger washing dishes a fox riding a bike a beetle riding a bike a fish riding a bike a dolphin riding a bike a rat riding a bike a frog playing chess a goose playing chess a turkey playing chess a camel playing chess a hedgehog playing chess	a horse washing dishes a zebra washing dishes a sheep washing dishes a goat washing dishes a bear washing dishes a wolf riding a bike a ant riding a bike a shark riding a bike a squirrel riding a bike a snake riding a bike a chicken playing chess a bee playing chess a fly playing chess a bat playing chess a kangaroo playing chess
Test list		
a cat riding a bike a dog playing chess a monkey riding a bike a rabbit playing chess a spider riding a bike a bird playing chess a deer riding a bike a cow playing chess a lion riding a bike a tiger playing chess a raccoon washing dishes a fox playing chess a lizard washing dishes a beetle playing chess a butterfly washing dishes a fish playing chess a whale washing dishes a dolphin playing chess a mouse washing dishes a rat playing chess a turtle washing dishes a frog riding a bike a duck washing dishes a goose riding a bike a pig washing dishes a turkey riding a bike a llama washing dishes a camel riding a bike a gorilla washing dishes a hedgehog riding a bike	a cat playing chess a horse riding a bike a monkey playing chess a zebra riding a bike a spider playing chess a sheep riding a bike a deer playing chess a goat riding a bike a lion playing chess a bear riding a bike a raccoon playing chess a wolf washing dishes a lizard playing chess a ant washing dishes a butterfly playing chess a shark washing dishes a whale playing chess a squirrel washing dishes a mouse playing chess a snake washing dishes a turtle riding a bike a chicken washing dishes a duck riding a bike a bee washing dishes a pig riding a bike a fly washing dishes a llama riding a bike a bat washing dishes a gorilla riding a bike a kangaroo washing dishes	a dog riding a bike a horse playing chess a rabbit riding a bike a zebra playing chess a bird riding a bike a sheep playing chess a cow riding a bike a goat playing chess a tiger riding a bike a bear playing chess a fox washing dishes a wolf playing chess a beetle washing dishes a ant playing chess a fish washing dishes a shark playing chess a dolphin washing dishes a squirrel playing chess a rat washing dishes a snake playing chess a frog washing dishes a chicken riding a bike a goose washing dishes a bee riding a bike a turkey washing dishes a fly riding a bike a camel washing dishes a bat riding a bike a hedgehog washing dishes a kangaroo riding a bike

Table 7. Prompt Lists for template 1.

Training list		
red apple brown banana red strawberry green grape brown kiwi yellow mango yellow pineapple yellow peach blue blueberry green raspberry green lime brown avocado red pomegranate red grapefruit	green apple orange orange green strawberry red watermelon green kiwi green pear brown pineapple purple plum purple blueberry yellow lemon yellow lime red cherry pink pomegranate	yellow banana yellow orange purple grape green watermelon orange mango yellow pear orange peach green plum red raspberry green lemon green avocado green cherry pink grapefruit
Test list		
yellow apple white strawberry white kiwi green pineapple black blueberry white lime white pomegranate white broccoli brown spinach white zucchini green garlic purple cauliflower white peas white brussels sprouts	green banana black grape green mango red peach black raspberry yellow avocado yellow grapefruit yellow tomato red lettuce white sweet potato white celery green eggplant green corn	green orange white watermelon brown pear red plum white lemon black cherry white carrot white cucumber yellow bell pepper green onion white cabbage purple asparagus purple green beans

Table 8. Prompt lists for template 2.

Training list		
chair under umbrella wheel on train tree under sky dog on boat person on street person on sofa table under vase building on the right of building kite on the right of kite road on the left of grass bowl on the right of plate bottle on the right of person car on the right of car person on the left of person	table under umbrella airplane on street building under sky tower under sky laptop on table glasses on face street under car suitcase on the left of person person on the left of ball grass on the right of road building on the right of truck box on the left of post truck on the right of car	car on street bag on street street under sky cup on shirt table under laptop sofa under person dog on the right of vase dog on the left of person ball on the right of person person on the left of pillow person on the left of bottle building on the left of building car on the left of car
Test list		
vase on table jacket on person person behind person trees behind grass truck in the front of building road under bus table under plate car on the right of umbrella bear on the right of person motorcycle on the left of bus	shirt on person motorcycle on road building behind trees wheel in the front of wheel cat in the front of vase road under building person under umbrella phone on the right of monitor bear on the left of person motorcycle on the left of car	watch on person motorcycle behind person hydrant behind motorcycle tower in the front of train trash can in the front of cabinet road under wheel cone on the right of cone person on the right of bear car on the left of bus road on the left of tree

Table 9. Prompt lists for template 3.